Available online at www.sciencedirect.com
SCIENCE DIRECT
Acta Materialia 54 (2006) 2181–2194
Acta MATERIALIA
www.actamat-journals.com

On the consideration of interactions between dislocations and grain boundaries in crystal plasticity finite element modeling – Theory, experiments, and simulations

A. Ma, F. Roters *, D. Raabe

Max-Planck-Institut für Eisenforschung, Max-Planck-Str. 1, 40237 Düsseldorf, Germany

Received 26 April 2005; received in revised form 6 January 2006; accepted 6 January 2006
Available online 10 March 2006

Abstract

We suggest a dislocation based constitutive model to incorporate the mechanical interaction between mobile dislocations and grain boundaries into a crystal plasticity finite element framework. The approach is based on the introduction of an additional activation energy into the rate equation for mobile dislocations in the vicinity of grain boundaries. The energy barrier is derived by using a geometrical model for thermally activated dislocation penetration events through grain boundaries. The model takes full account of the geometry of the grain boundaries and of the Schmid factors of the critically stressed incoming and outgoing slip systems and is formulated as a vectorial conservation law. The new model is applied to the case of 50% (frictionless) simple shear deformation of Al bicrystals with either a small, medium, or large angle grain boundary parallel to the shear plane. The simulations are in excellent agreement with the experiments in terms of the von Mises equivalent strain distributions and textures. The study reveals that the incorporation of the misorientation alone is not sufficient to describe the influence of grain boundaries on polycrystal micro-mechanics. We observe three mechanisms which jointly entail pronounced local hardening in front of grain boundaries (and other interfaces) beyond the classical kinematic hardening effect which is automatically included in all crystal plasticity finite element models owing to the change in the Schmid factor across grain boundaries. These are the accumulation of geometrically necessary dislocations (dynamic effect; see [Ma A, Roters F, Raabe D. A dislocation density based constitutive model for crystal plasticity FEM including geometrically necessary dislocations. Acta Mater 2006;58:2169–79]), the resistance against slip penetration (dynamic effect; this paper), and the change in the orientation spread (kinematic effect; this paper) in the vicinity of grain boundaries.

Keywords: Dislocation density; Grain boundary mechanics; Grain boundary element; Slip penetration; Aluminum

1. Introduction

Different types of experiments such as micro-torsion, micro-bending, deformation of particle-reinforced metal–matrix composites, and micro-indentation hardness tests have revealed similar hardening effects when refining the deformation scale, substantiating a general length scale dependence of the flow stress [2]. The common feature of these experiments is that the non-uniform plastic deformation imposed in such cases entails the formation of orientation gradients among neighboring material points and, hence, the accumulation of extra dislocations for the preservation of the lattice continuity.

In order to integrate these various interconnected aspects into one constitutive model, we introduce in Ref. [1] and in this study a joint formulation which includes the tensorial nature of elastic–plastic deformation in terms of dislocation slip, the evolution of the crystallographic texture at each material point, nonlocal orientation- and strain-gradient terms occurring between neighboring material points, and the local mechanical effects associated with interfaces. The aim is to provide a general framework for

* Corresponding author. Tel.: +49 211 6792 393; fax: +49 211 6792 333.
E-mail address: roters@mpie.de (F. Roters).

1359-6454/$30.00
doi:10.1016/j.actamat.2006.01.004

studying polycrystal micro-mechanics at small spatial scales in a crystal-plasticity finite element framework. The central problem addressed in this paper is the local effect of grain boundaries on the hardening behavior. The general introduction of geometrically necessary dislocations into the crystal plasticity finite element framework has been discussed in Ref. [1].

A basic issue associated with the constitutive aspects discussed above is the description of the constraints imposed by the neighborhood on one particular material point.

In finite element simulations which use empirical local constitutive models the relation between a material point and its neighborhood is satisfied by accounting for the equilibrium of the forces and the continuity of the total deformation, and, of course, the procedure of solving the boundary value problem satisfying these constraints.

For approaches which add nonlocal terms to an otherwise local dislocation model in the bulk crystal, Nye's dislocation tensor [3] can be used to express the constraints imposed by the neighborhood on a material point. This is due to the fact that orientation differences between neighboring points which are far away from rigid obstacles are usually small. The accumulation of geometrically necessary dislocations then acts as a penalty term against local reorientations entailing a resistance against the formation of orientation gradients upon loading. In such cases we encounter three constraint conditions in the boundary value problem, namely, the two constraints mentioned above plus the accommodation of the lattice curvature in terms of Nye's dislocation tensor.

When additionally considering the slip resistance associated with slip penetration events across grain boundaries the influence among neighboring material points becomes more complex. In such a case the total set of conditions are the three constraints mentioned above plus the transmission (penetration), reflection, and absorption of mobile dislocations by grain boundaries including the tensorial and structural nature of that problem.

The latter aspect is central in this study. The approach that we choose is the introduction of a grain boundary transmission mechanism, which is added to the nonlocal dislocation model introduced in the preceding study [1]. The transmission mechanism enters through an additional activation enthalpy term which quantifies the penetration probability of mobile dislocations through grain boundaries. The activation enthalpy is the elastic energy of formation of misfit dislocations which remain as debris in the interface upon slip penetration. This new energy barrier is introduced in the form of a special grain boundary element which contains the actual interface.

In order to critically evaluate the new model we conduct corresponding simulations of simple shear deformation tests of pure aluminum bicrystals with different grain boundaries (small angle, 7.4°; medium angle, 15.9°; large angle, 33.2° [4]). The grain boundary plane is in all cases parallel to the shear plane. The predictions are compared to experiments (50% shear) in terms of the von Mises equivalent strain distributions, the statistical orientation distributions, and the local textures on the sample surface. The constitutive parameters required for the constitutive dislocation model are fitted by approximating the average stress–strain curve of a single crystal as outlined in Ref. [1].

2. Grain boundary micro-mechanics observed in earlier experiments

Grain boundaries act as obstacles to the motion of dislocations. At the onset of plastic deformation of polycrystals, mobile dislocations are first created on the slip system with the largest local resolved shear stress in the grain with the most favorable orientation. When encountering a grain boundary, such mobile dislocations will accumulate in the form of pile-ups entailing a local stress state which can be approximated by a super dislocation. At the tip of that pseudo dislocation stress concentrations arise which add to the external stress field at this material point. Such micro-plastic effects, where the local arrangement of dislocations plays the dominant role for the local stress, cannot be mapped one-to-one by crystal plasticity-type continuum mechanics which map dislocation mechanics in a phenomenological statistical or even in an empirical fashion. However, homogenization is admissible at larger plastic strains where most of the slip activation processes can be captured by long-range stresses rather than by local ones [5]. This means that dislocation mechanics can, beyond the microplastic regime, be homogenized in the form of statistical dislocation populations which in turn can be embedded as constitutive rate equations in a crystal plasticity theory [1,6,7]. The basic applicability of the crystal plasticity finite element approach to a large spectrum of intricate micromechanical problems has been shown by many studies in which both the textures and the strains were properly predicted when compared to corresponding experiments [4,8–13].

At very low plastic strains where isolated dislocation pile-ups can be observed [5], careful studies in the vicinity of grain boundaries by transmission electron microscopy showed several types of interactions between the mobile dislocations and the interface. These are the direct transmission or penetration of dislocations through grain boundaries, the reflection of dislocations at grain boundaries, and the absorption of dislocations into grain boundaries [14,15]. Among these interactions, the slip penetration (transmission) especially has been shown to provide a very important contribution to the deformation of polycrystalline materials. Based on the experimental data obtained at very small plastic strains, Livingston and Chalmers [16], Clark et al. [5] and Lee et al. [17] have proposed several criteria for the penetration of slip through a grain boundary. These criteria include the relationship between the Burgers vectors on either side of an interface, the interaction lines between the grain boundary and the slip planes of the incoming and outgoing dislocations, the resolved shear stress on the outgoing side related to the stress field of the pile-up dislocations on the incoming side, and

residual grain boundary dislocations left as debris in the interface during a transmission event.

Livingston and Chalmers [16], Clark et al. [5] and Lee et al. [17] suggest that, if a slip penetration event occurs at a grain boundary, the criteria outlined above can be used to determine the expected outbound dislocations for a given set of inbound ones. We apply these criteria as guidelines for the identification of those mechanisms which should enter into an improved crystal plasticity finite element model for the incorporation of grain boundary micro-mechanics in a constitutive framework which is based on the dislocation model developed in Ref. [1].

3. Discussion of grain boundary micro-mechanics in conjunction with crystal plasticity finite element theory

In this section, we discuss various approaches which are conceivable for the introduction of grain boundary micro-mechanics into a crystal plasticity finite element constitutive framework.

3.1. Energy equivalence concept

A first possible concept for including grain boundaries in a crystal plasticity finite element (FE) model consists in using the grain boundary energy as an approach for introducing an interface resistance against slip penetration in terms of geometrically necessary dislocations. The idea behind this approach is to directly translate the grain boundary energy [18] into a generalized Read–Shockley-type formulation and by using this form for extracting an equivalent density of geometrically necessary dislocations which replaces the actual grain boundary in a finite element which carries the interface properties. This approach suffers from two drawbacks: First, we could not identify a suited homogenization model which acts locally. This means that it is unclear how such equivalent dislocations would act as a barrier and interfere with the motion of the mobile dislocations according to the basic framework outlined in Ref. [1]. Second, such an approach does not include the tensorial nature of the problem. This means that a robust micro-mechanical concept of the grain boundary as an obstacle against dislocation motion requires that the slip resistance encountered by mobile dislocations must be different for different incoming and outgoing glide systems (which are described by three orthogonal vectors, namely, the glide vector $\mathbf{d}^{\alpha}$, the line or tangent vector $\mathbf{t}^{\alpha}$ and the slip plane normal vector $\mathbf{n}^{\alpha}$). Examples at hand are easy grain boundary transmission events, such as are conceivable for small angle grain boundaries or certain coherent twin interfaces [5,14,15,19], as opposed to difficult penetration events, such as in the case for large angle grain boundaries with large CSL (coincidence site lattice) numbers and a large misalignment between the slip systems on either side. A locally enhanced equivalent scalar density of geometrically necessary dislocations cannot reflect such tensorial physics of slip penetration.

3.2. Misorientation equivalence concept

A second possible concept is to directly use Nye's dislocation tensor [3] for mapping the micro-mechanics of grain boundaries. This approach amounts to using the respective misorientation associated with a grain boundary instead of its energy to derive an equivalent density of geometrical dislocations. The disadvantage of this approach is that Nye's theory is built on small orientation gradients which would exclude the possibility of mapping the nature of large angle grain boundaries. Also, grain boundaries represent lattice defects the structure of which may change discontinuously as a function of the misorientation. While grain boundaries can in the small angle regime be well described by the Read–Shockley concept [20], large angle grain boundaries do not consist of lattice dislocations. This means that Nye's tensor does not apply for large angle grain boundaries since they do not contain, in the unstrained state, any geometrically necessary dislocations within their actual grain boundary area but consist rather of relaxed structural units which do not form lattice dislocations [19]. A continuous and dislocation based description of grain boundaries with arbitrary misorientation in terms of Nye's dislocation tensor is, therefore, a less pertinent concept to capture grain boundary micro-mechanics in a crystal plasticity FE environment. Another drawback associated with a continuous Nye-type model of grain boundary mechanics is the tensorial nature of the problem: The translation of a local orientation difference of two abutting crystals directly into geometrically necessary dislocation populations does not give a unique solution, since different combinations of slip systems could yield the same result. The details associated with these initial values of the local densities of geometrically necessary dislocations are, however, important for the very beginning of plastic deformation.

3.3. Thermally activated slip transmission concept

In the following we give an outline of a third way to approach the problem.

The transmission probability of incoming mobile dislocations which try to penetrate a grain boundary can be treated in terms of an activation concept. The enthalpy for this activation process stems from the elastic energy of formation of potential misfit dislocations which would remain as debris in the interface upon slip penetration. This activation enthalpy enters as an additional contribution into the activation term for the slip of mobile dislocations (see details of the constitutive equations in Refs. [1] or [21]). It is likely that each transmission event will occur at the smallest possible energy consumption which provides a natural selection criterion for the outgoing slip system, when the incoming one is known.

If we describe the inbound slip system in the first grain by the shear vector $\mathbf{d}^{\alpha}$, the tangent vector $\mathbf{t}^{\alpha}$, and the slip plane normal vector $\mathbf{n}^{\alpha}$, the task consists of identifying that

particular abutting (outbound) slip system on the other side of the boundary $(\mathbf{d}^{\beta},\mathbf{t}^{\beta},\mathbf{n}^{\beta})$ which provides the minimum energy barrier, i.e., the smallest misalignment relative to the active inbound slip system. We do not actually check whether or not this slip system on the other side of the grain boundary can be truly activated by the local stress but assume in a somewhat simplifying fashion, that its activation is possible, as the slip system orientation is close to the inbound one. For an arbitrary transmission event, it is obvious that some incoming slip system does as a rule not match a corresponding one on the outbound side, i.e., a geometrically coherent shear system on the other side of the grain boundary. Therefore, in order to meet the conservation of the lattice defect vector sum when crossing an interface, certain misfit dislocations will be left in the grain boundary. The additional energy required to produce such an extra misfit dislocation acts as an energy barrier measure for this thermally activated slip transmission event.

One should emphasize that this transmission event provides a method to quantify the penalty energy required for such an event. However, as we are modeling the material behavior on a homogenized continuum scale there need not be a strict one-to-one correlation between incoming and outgoing dislocations. Moreover, it is conceivable that the transmission only rarely takes place owing to the local hardening effect that it introduces and that, instead, the accumulation of geometrically necessary dislocations increases the stiffness locally. These aspects will be discussed in detail in Section 6. A final remark concerns the misfit dislocations. While they serve as a means to quantify the penalty energy they will very likely not be stored but be dissolved by some relaxation process in the grain boundary. This implies that there will be no accumulation of misfit dislocations in the boundary, which would alter the process for newly incoming dislocations. Moreover, the assumption that the general character of the grain boundary is not altered by the penetration process allows us to use the same model of the penetration process for small strains and large strains.

4. A grain boundary micro-mechanical mechanism based on dislocation transmission

In this chapter, we discuss the mathematical treatment of the third possibility for treating the grain boundary effect as discussed in the previous chapter.

We consider two crystals with orientations $\mathbf{Q}_{\mathrm{I}}$ and $\mathbf{Q}_{\mathrm{II}}$ with slip systems $(\mathbf{d}^{\alpha,\beta},\mathbf{t}^{\alpha,\beta},\mathbf{n}^{\alpha,\beta})$, $\alpha,\ \beta=1,2,\ldots,12$,[1] and a grain boundary with a normal vector $\mathbf{n}_{\mathrm{GB}}$, which separates these two crystals, see Fig. 1.

According to Fig. 1(a), we assume that the dislocation line elements, $\mathbf{l}^{\alpha}$ and $\mathbf{l}^{\beta}$, will align with the boundary plane during the transmission event. This means that we use the two line elements:

$$\mathbf{l}^{\alpha'}=l^{\alpha}(\mathbf{n}_{\mathrm{GB}}\times\mathbf{n}^{\alpha}) \tag{1}$$

$$\mathbf{l}^{\beta'}=l^{\beta}\left(\mathbf{n}_{\mathrm{GB}}\times\mathbf{n}^{\beta}\right) \tag{2}$$

instead of $\mathbf{l}^{\alpha}$ and $\mathbf{l}^{\beta}$ for the conservation law of the lattice defect (expressed by the dislocation tensor) during the penetration event

$$\mathbf{b}^{\alpha}\otimes\mathbf{l}^{\alpha'}=\mathbf{b}^{\beta}\otimes\mathbf{l}^{\beta'}+\mathbf{b}^{\alpha}_{\mathrm{GB}}\otimes\mathbf{l}^{\alpha}_{\mathrm{GB}} \tag{3}$$

where $\mathbf{b}$ is the respective Burgers vector and the index GB refers to the grain boundary dislocation, i.e., to the debris which remains in or at the grain boundary upon slip penetration.

The energy of formation for these misfit dislocations fulfills the following inequality:

$$\frac{1}{2}Gb^{2}l^{\alpha'}\leqslant\frac{1}{2}Gb^{2}l^{\beta'}+\frac{1}{2}Gb_{\mathrm{GB}}^{\alpha^{2}}l^{\alpha}_{\mathrm{GB}} \tag{4}$$

where G is the shear modulus. As both mobile dislocations in grains I and II are crystal dislocations, we assume that they have equal energies. Therefore, the additional energy for the transmission event is the energy of formation of the grain boundary dislocation which has to be formed during the process. The final task is to identify for every slip system α of crystal I a slip system β in crystal II with the boundary condition that the energy of the grain boundary dislocation is minimized upon slip transmission

$$E^{\alpha}_{\mathrm{GB}}=\min_{\beta}\frac{1}{2}Gb_{\mathrm{GB}}^{\alpha^{2}}l^{\alpha}_{\mathrm{GB}} \tag{5}$$

We now have to determine $\mathbf{b}^{\alpha}_{\mathrm{GB}}$ and $\mathbf{l}^{\alpha}_{\mathrm{GB}}$ in such a way that Eq. (3) is fulfilled. However, as we are interested in the activation energy only, it is sufficient to determine the magnitude of the vectors, i.e., b^{α}_{GB} and l^{α}_{GB}. This means that we can rewrite Eq. (3):

$$\|\mathbf{b}^{\alpha}_{\mathrm{GB}}\otimes\mathbf{l}^{\alpha}_{\mathrm{GB}}\|=\|\mathbf{b}^{\alpha}\otimes\mathbf{l}^{\alpha'}-\mathbf{b}^{\beta}\otimes\mathbf{l}^{\beta'}\| \tag{6}$$

which can be reformulated into

$$\|\mathbf{b}^{\alpha}_{\mathrm{GB}}\|\|\mathbf{l}^{\alpha}_{\mathrm{GB}}\|=\|\mathbf{b}^{\alpha}\otimes\mathbf{l}^{\alpha'}-\mathbf{b}^{\beta}\otimes\mathbf{l}^{\beta'}\| \tag{7}$$

This expression does not have a unique solution. Whenever identifying a pair of $\|\mathbf{b}^{\alpha}_{\mathrm{GB}}\|$ and $\|\mathbf{l}^{\alpha}_{\mathrm{GB}}\|$ that satisfies Eq. (7) any pair $c\|\mathbf{b}^{\alpha}_{\mathrm{GB}}\|$ and $\frac{1}{c}\|\mathbf{l}^{\alpha}_{\mathrm{GB}}\|$ with c being an arbitrary constant would also be a valid solution. However, when using Eq. (5) to calculate E^{α}_{GB} the result would change by a factor c.

Nevertheless, when fixing, for example, the magnitude of $\mathbf{b}^{\alpha}_{\mathrm{GB}}$ to cb, where b is the magnitude of the lattice Burgers vector, one can calculate $\|\mathbf{l}^{\alpha}_{\mathrm{GB}}\|$ as

$$l^{\alpha}_{\mathrm{GB}}=\frac{1}{cb}\|\mathbf{b}^{\alpha}\otimes\mathbf{l}^{\alpha'}-\mathbf{b}^{\beta}\otimes\mathbf{l}^{\beta'}\| \tag{8}$$

and the energy for the activation event can be calculated as

$$E^{\alpha}_{\mathrm{GB}}=\min_{\beta}c^{2}\frac{1}{2}Gb^{2}l^{\alpha}_{\mathrm{GB}} \tag{9}$$

When further writing the length of l^{α}_{GB} in multiples of the magnitude of the lattice Burgers vector, that is

[1] The indices α and β always refer to crystals I and II, respectively.

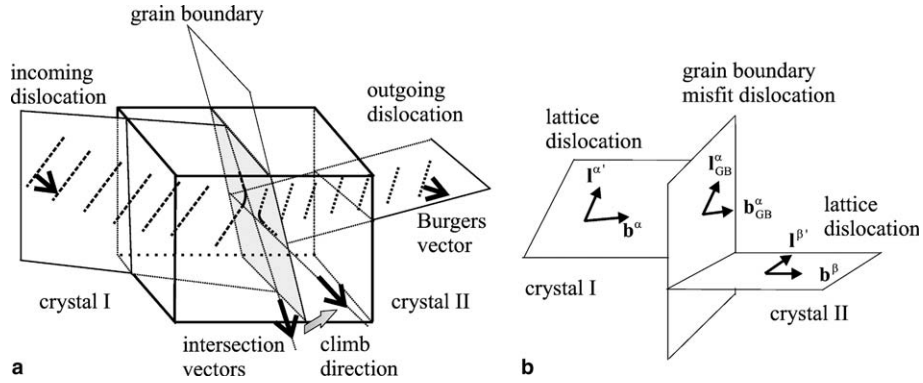

Fig. 1. Schematic drawing of penetration events for mobile dislocations through a grain boundary. $\mathbf{l}^{\alpha'}$, $\mathbf{l}^{\beta'}$, $\mathbf{l}^{\alpha}_{GB}$ are the line vectors, and $\mathbf{b}^{\alpha}$, $\mathbf{b}^{\beta}$, $\mathbf{b}^{\alpha}_{GB}$ are the Burgers vectors of the dislocations in the moment of the penetration event. α and β indicate crystals I and II and the index GB the grain boundary dislocation.

$$l^{\alpha}_{GB} = ab \tag{10}$$

where a is determined by Eq. (8) we finally obtain

$$E^{\alpha}_{GB} = \min_{\beta} c^2 a \frac{1}{2} Gb^3 \tag{11}$$

It is worthwhile mentioning at this point, that while the absolute magnitude of E^{α}_{GB} can be changed by the choice of c, the ratio of the activation energies for different boundaries is not affected by this value.[2]

The activation energies of an incoming dislocation with length b are calculated for twist boundaries with rotations about the [1 1 1] and [1 1 0] crystal directions for the face-centred cubic crystal structure under the additional constraint, that the grain boundary plane is perpendicular to these rotation axes. The results are shown in Figs. 2 and 3, where the activation energy has been normalized by the factor $\frac{1}{2}Gb^3$ and the constant c was chosen to be equal to one. Both figures also show the average of the energy barrier for better comparison. From these curves, it is clear that a grain boundary is a strong obstacle to dislocation motion, as the average activation energies for the formation of the misfit dislocations reach the order of magnitude of the activation energy for forest cutting.

It can be seen that the energies for slip penetration show a periodic behavior. This periodicity arises from the octahedral symmetry of the slip systems in the crystal. Every change in the choice of the outgoing slip system β causes a discontinuous change in the slope of the energy curve. One can see that the energy barrier strongly depends on the misorientation of the two crystals, especially when the rotation angle is larger than about 20°. However, the average activation energies show a much more constant behavior than the single slip system curves suggest, which implies that the strong effect for individual slip systems will be averaged out to some extent in macroscopic experiments.

[2] c, therefore, serves as a fitting parameter in the model.

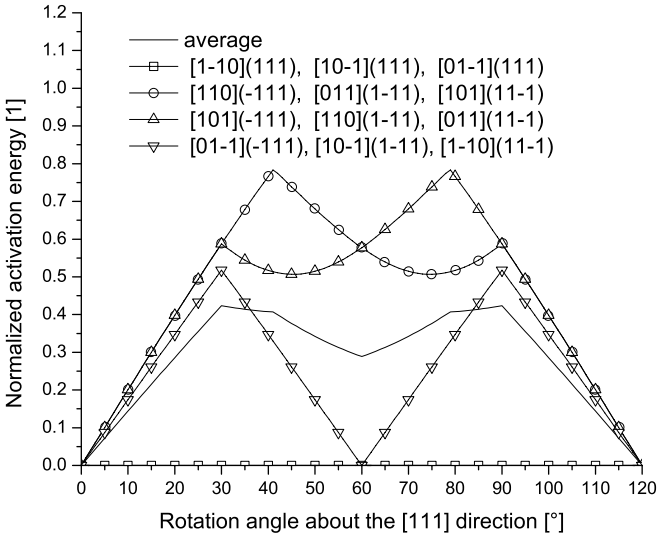

Fig. 2. Normalized activation energy for twist grain boundaries with rotation about the [1 1 1] direction using $c = 1$ in Eq. (11), the normalization factor is $\frac{1}{2}Gb^3$.

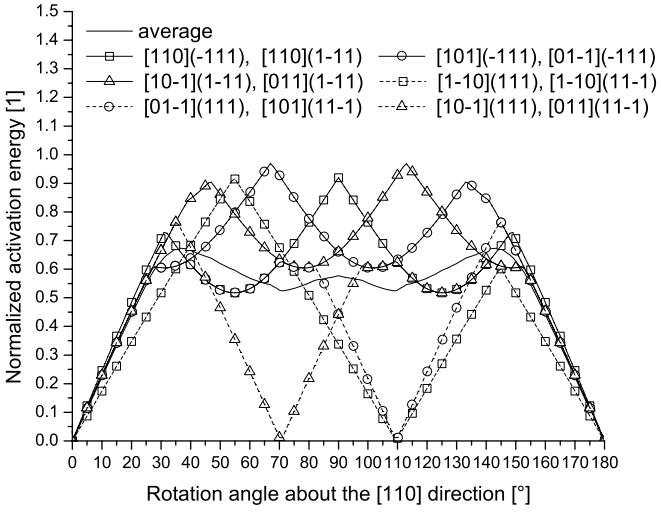

Fig. 3. Normalized activation energy for twist grain boundaries with rotation about the [1 1 0] direction using $c = 1$ in Eq. (11). The normalization factor is $\frac{1}{2}Gb^3$.

Finally one has to consider two special situations: first, when the grain boundary plane is parallel to the slip plane of the incoming dislocation the energy barrier is set to zero, because the mobile dislocations do not penetrate the grain boundary, but they move parallel to it; second, when the plane of the outgoing dislocation is parallel to the grain boundary we set $\mathbf{l}^{\beta'}$ parallel to $\mathbf{l}^{\alpha'}$ as there is no intersection line with the grain boundary.

In summary the new model developed in this paragraph assigns an obstacle strength of the grain boundary which does not only depend on the grain boundary misorientation but also on the grain boundary plane orientation ($\mathbf{n}_{GB}$) and on the slip systems involved on either side of the interface.

5. The grain boundary element

In all crystal plasticity FE modeling (FEM) implementations known to the authors the grain boundaries coincide with element boundaries. In contrast to this approach we use a grain boundary implementation in the form of a special grain boundary element. In this element we use a modified version of the flow rule given in Ref. [1], namely

$$\dot{\gamma}^{\alpha} = \begin{cases} \dot{\gamma}_0^{\alpha} \exp\left[-\frac{Q_{\text{eff}}}{k_B\theta}\left(1-\frac{|\tau^{\alpha}|-\tau^{\alpha}_{\text{pass}}}{\tau^{\alpha}_{\text{cut}}}\right)\right]\text{sign}(\tau^{\alpha}) & |\tau^{\alpha}| > \tau^{\alpha}_{\text{pass}} \\ 0 & |\tau^{\alpha}| \leqslant \tau^{\alpha}_{\text{pass}} \end{cases} \tag{12}$$

where the pre-exponential variable $\dot{\gamma}_0^{\alpha}$ and passing stress $\tau^{\alpha}_{\text{pass}}$ are the same as equations 15 and 16 in Ref. [1]. The cutting stress caused jointly by the forest dislocations and the grain boundary at 0 K now reads

$$\tau^{\alpha}_{\text{cut}} = \frac{Q_{\text{eff}}}{c_2 c_3 b^2}\sqrt{\rho^{\alpha}_{\text{F}}} \tag{13}$$

where c_2 and c_3 are again constants and Q_{eff} is the modified effective activation energy:

$$Q_{\text{eff}} = Q_{\text{slip}} + Q^{\alpha}_{\text{GB}} \tag{14}$$

When comparing this flow rule with the one specified in Ref. [1], the only difference is the use of Q_{eff} instead of Q_{slip}. The energy Q^{α}_{GB} is calculated according to Eq. (11) as

$$Q^{\alpha}_{\text{GB}} = \min_{\beta} c_9 a \frac{1}{2} G b^3 \tag{15}$$

with the constant $c_9 = c^2$.

Modifying the activation energy for an individual dislocation jump in Eq. (12) implies that the boundary is overcome in a single activation event.

The activation area for this event is of the order $\lambda^{\alpha} b$. In this expression λ^{α} is the trapping length of the mobile dislocation (see Fig. 4(a)) and b is the magnitude of the lattice Burgers vector, which is used as the obstacle width for the piercing dislocation density. However, when simply adding the activation energies, we use the same activation area for the transmission event. Therefore, when

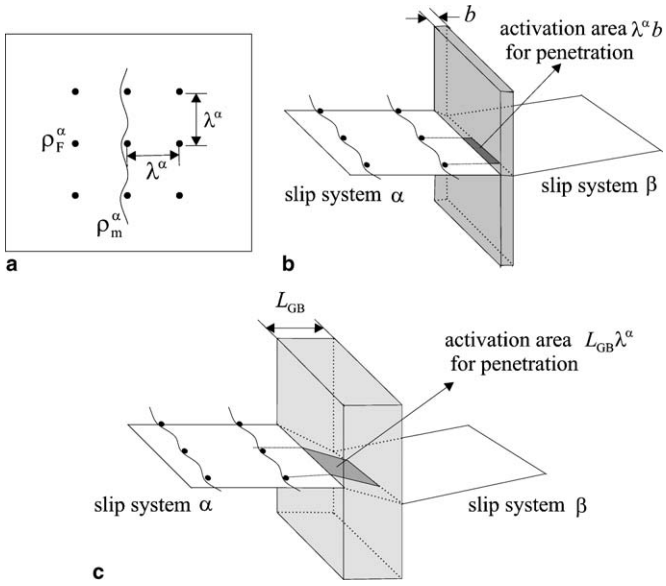

Fig. 4. Schematic drawing of the penetration and cutting mechanism: (a) cutting mechanism; (b) penetration of perfect grain boundary; (c) FEM treatment of penetration process; ρ^{α}_{m} is the density of mobile dislocations for slip system α, ρ^{α}_{F} the density of forest dislocations, λ^{α} the average obstacle spacing, and L_{GB} the thickness of the grain boundary element.

adopting a in Eq. (11) in such a way that the length of the transmitted dislocations equals λ^{α}, the element thickness of the boundary element should amount to a value close to b (see Fig. 4(b)). If we further assume that we start with a mesh of brick elements the element volume ($b\lambda^{\alpha}\lambda^{\alpha}$) would be of the order of 1 μm^3 or less. Even if we use small samples in the mm size range, this would mean that we need about one billion elements to mesh our sample. This number is too high for practical applications.

The only way to circumvent this problem is to increase the element thickness to L_{GB} (Fig. 4(c)). However, by doing so we assign an overly stiff material behavior to a volume much bigger than the actual grain boundary volume. In order to compensate for this large volume we can artificially decrease the grain boundary strength by the choice of the constant $c_9 \propto \frac{b}{L_{\text{GB}}}$. It has to be stressed though, that this is a purely empirical adjustment due to the use of larger finite elements and does not describe the scaling of the underlying physics one-to-one.

6. Simple shear tests

The grain boundary model introduced in this paper is implemented in the commercial finite element code MSC.Marc200x in terms of the user defined material subroutine HYPELA2 [22]. The experimental setup and the boundary conditions are described in Ref. [1]. The only difference is that for the bicrystal simulations quoted in this paper, each set of four integration points on either side of the interface in the newly introduced grain boundary elements shown in Fig. 5 carries the initial orientations of the

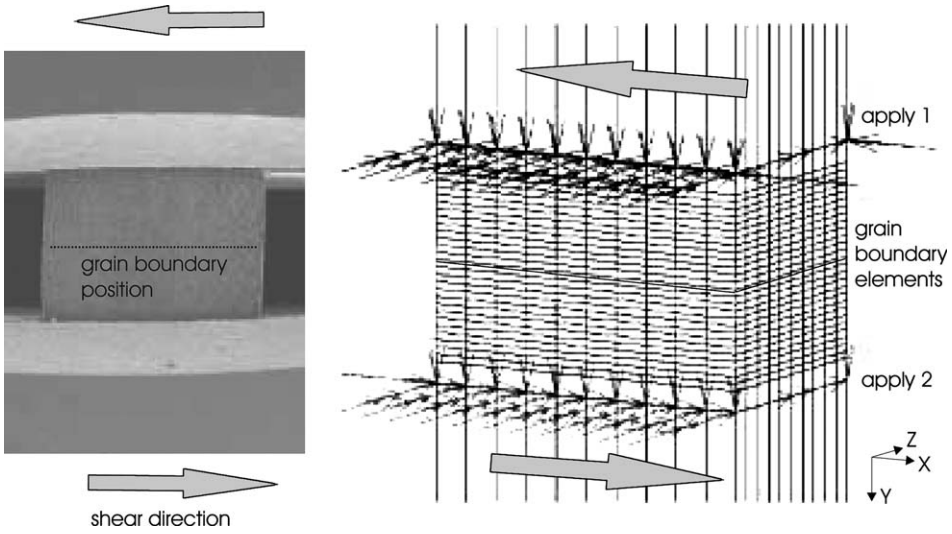

Fig. 5. Experimental setup and finite element mesh used for the simulations indicating also the boundary conditions applied. The grain boundary elements are highlighted.

abutting crystals. In such elements, which initially contain a change in crystal orientation within their element borders according to the real bicrystal, the new constitutive grain boundary law is applied resulting in a locally increased stiffness in terms of an additional energy barrier for each incoming slip system as outlined above.

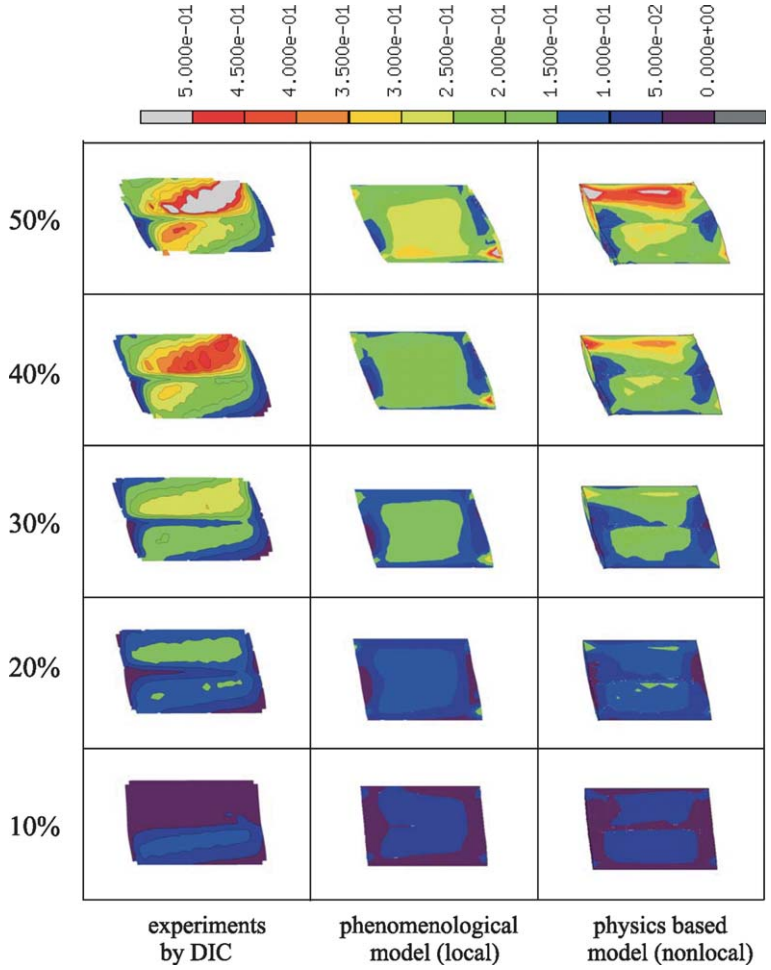

Fig. 6. Simple shear test of a bicrystal (3.1 mm long, 2.0 mm thick and 2.2 mm high) with a low angle grain boundary (7.4°). Comparison of the von Mises strain patterns of the experiment obtained by digital image correlation (DIC, left column), from the simulation with a conventional viscoplastic constitutive law (middle column), and from the simulation which uses the new set of constitutive laws (right column).

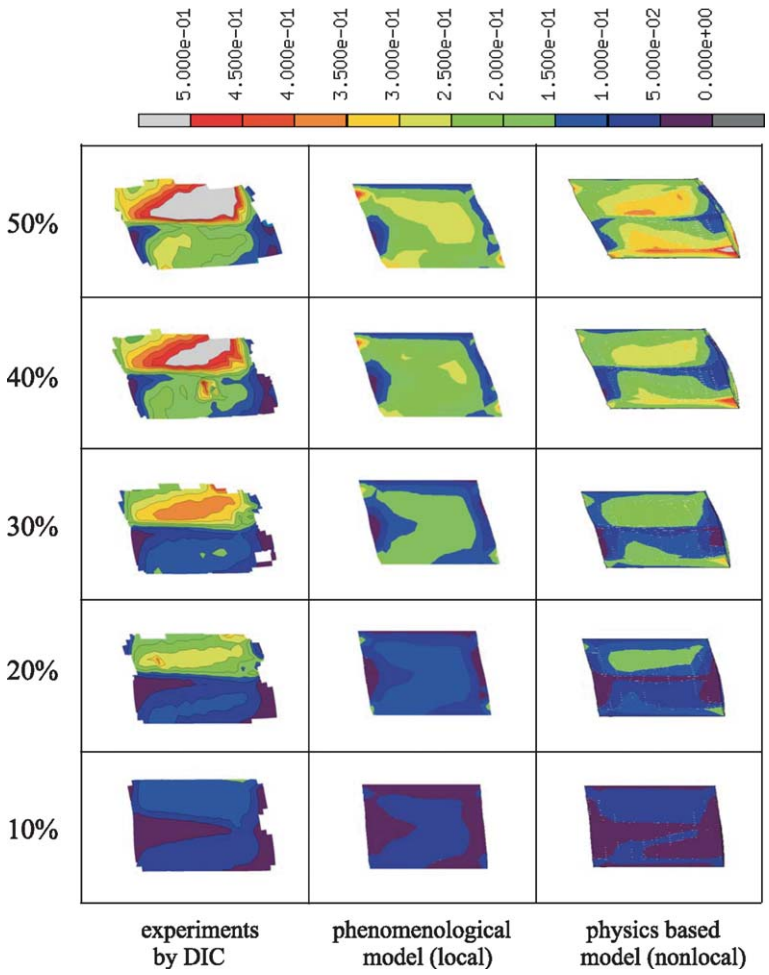

Fig. 7. Simple shear test of a bicrystal (3.1 mm long, 2.0 mm thick and 2.2 mm high) with a medium angle grain boundary (15.9°). Comparison of the von Mises strain patterns of the experiment obtained by digital image correlation (DIC, left column), from the simulation with a conventional viscoplastic constitutive law (middle column), and from the simulation which uses the new set of constitutive laws (right column).

6.1. Simple shear tests for aluminum bicrystals

The same constitutive parameters which were fitted with the help of the single crystal simple shear tests in Ref. [1] were used for simulations of three bicrystal shear tests. The first bicrystal had a 7.4° small angle grain boundary with the initial orientations $(\varphi_1 = 277.0°,\ \Phi = 32.3°,\ \varphi_2 = 37.4°)_{\mathrm{I}}$ and $(\varphi_1 = 264.7°,\ \Phi = 32.3°,\ \varphi_2 = 44.3°)_{\mathrm{II}}$. The second bicrystal had a 15.9° grain boundary with the initial orientations $(\varphi_1 = 74.3°,\ \Phi = 37.1°,\ \varphi_2 = 50.1°)_{\mathrm{I}}$ and $(\varphi_1 = 87.9°,\ \Phi = 36.7°,\ \varphi_2 = 52.9°)_{\mathrm{II}}$. The third bicrystal had a 33.2° grain boundary with the initial orientations $(\varphi_1 = 105.9°,\ \Phi = 34.1°,\ \varphi_2 = 43.4°)_{\mathrm{I}}$ and $(\varphi_1 = 64.1°,\ \Phi = 34.8°,\ \varphi_2 = 54.6°)_{\mathrm{II}}$ [23]. All three bicrystals have a planar symmetric tilt grain boundary with the [1 1 2] crystal direction as common tilt axis which is parallel to the Y axis (TD direction of the finite element mesh, see Fig. 5).

6.1.1. Comparison of the accumulated plastic strain

Figs. 6–8 show the comparison of the von Mises strain patterns obtained from the experiment (left column), from the simulation with a conventional viscoplastic constitutive law (middle column), and from the simulation series which is based on the new set of constitutive laws including dislocation rate formulations on each slip system, geometrically necessary dislocations on each slip system, and a geometrical model for the grain boundary resistance against slip transmission events as introduced in this work (right column). The figures show the von Mises equivalent strain distributions for five subsequent stages of shear with a constant increase of 10% per load step.

The experimental data clearly reveal in all three cases the strong micro-mechanical effect imposed by the presence of the respective grain boundaries.

Even for the small angle grain boundary (7.4°) the shear experiment shows an effect of strain separation among the two abutting crystals. With increasing grain boundary misorientation the heterogeneous distribution of the von Mises strain becomes more pronounced.

The experimental results are different from those reported earlier in Ref. [4,23] where channel-die tests were used for deforming a set of similar bicrystals. These

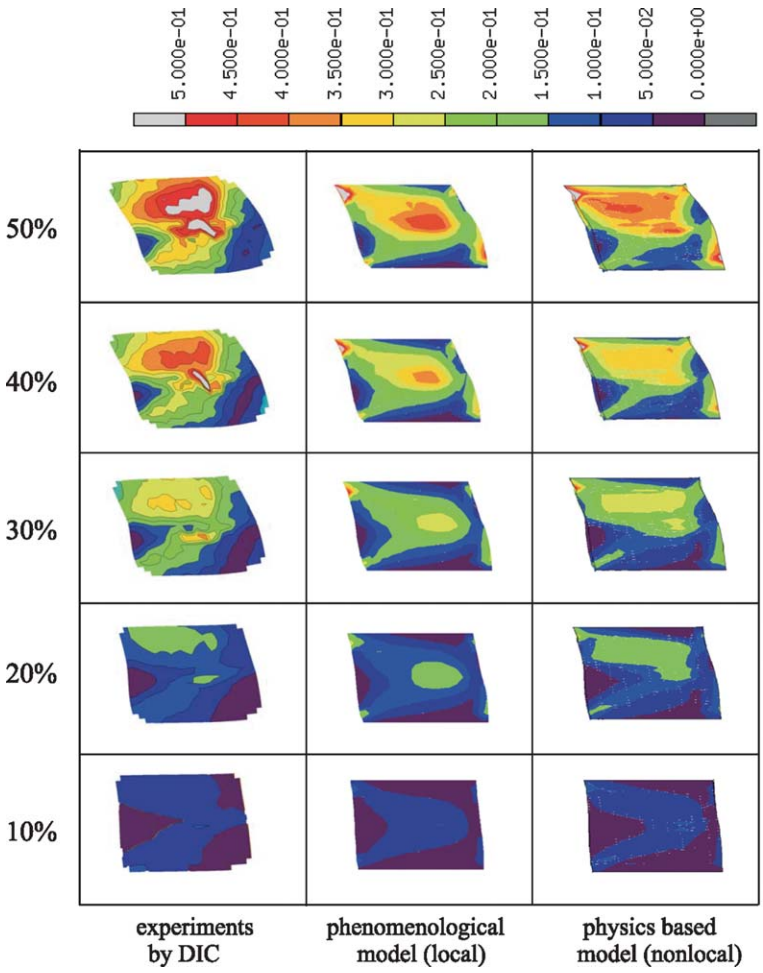

Fig. 8. Simple shear test of a bicrystal (3.1 mm long, 2.0 mm thick and 2.2 mm high) with a large angle grain boundary (33.2°). Comparison of the von Mises strain patterns of the experiment obtained by digital image correlation (DIC, left column), from the simulation with a conventional viscoplastic constitutive law (middle column), and from the simulation which uses the new set of constitutive laws (right column).

earlier experiments revealed a disturbing influence of friction and of the length to height ratio of the specimens so that the mechanical effect arising from the presence of interfaces was overlapped by these macro-mechanical effects.

Also, in the channel-die experiments the load was imposed in a symmetrical fashion and the symmetry of the plane strain state relative to the initial orientations of the two abutting crystals produced a weak mirror symmetry during plastic deformation in the RD–ND plane. This effect is avoided in our current shear experiments.

A further reason for the absence of symmetry effects in the shear experiments is the non-linear material behavior resulting from the highly non-linear flow and hardening rules which may yield very different results even for tiny deviations in the initial state or in the local boundary conditions.

The complicated cross-hardening effect may also contribute to the absence of symmetry. Probably the most important influence for the absence of strain symmetry, however, are micro-mechanical effects arising from the presence of the grain boundaries. The experimental data reveal that in all three bicrystals one of the two abutting crystals accumulates more plastic strain when compared to the other.

Concerning the corresponding simulation results it is essential to note that the use of the empirical viscoplastic (local) law (second rows of Figs. 6–8) does not adequately reproduce the influence of the grain boundaries on the lateral distribution of the accumulated von Mises strain. This applies in particular to the two bicrystals which have a small and medium angle grain boundary, respectively. For the bicrystal with the large angle grain boundary, Fig. 8, the empirical (local) model is capable to predict some although not all characteristics of the strain separation between the two crystals. This partial success of the simulation with the empirical viscoplastic hardening law in case of the large angle grain boundary is attributed to the strong effect of the change in the Schmid factor across the interface. This means that the kinematic effect which arises from distinct differences in the slip system selection on either side of a grain boundary plays an essential role in this case. We refer to this effect as kinematic hardening imposed by grain boundaries.

The simulation results obtained by using the new model match the experimental data much better. For the bicrystals with the small angle grain boundary and that with the large angle grain boundary, one grain is deformed more significantly than the other which reproduces the experimental observation very well. The predictions for the bicrystal with the medium angle grain boundary, Fig. 7, show some deviations to the experimental findings. In order to analyse possible reasons for this deviation we present a section through the predicted equivalent total strain map in the ND–TD plane of the mesh near the corner of the sample in Fig. 9.

The section reveals that the cross-section of the specimen near the corner point shrinks considerably compared to the undeformed sample shape. In the experiment the external load is imposed via friction between the sample surface and the tool under strong external pressure. During the deformation experiment the sample detaches partially from the clamping tool, Fig. 9(d), due to the shrinking process.

Although the specimen experiences the same tendency to change its shape locally in the finite element simulations the boundary conditions imposed (Fig. 5) do not allow for detachment. This gives rise to artificially large stretches in this area, Fig. 9(c). We, therefore, attribute the small deviations between the experiment and the simulation with the new nonlocal model observed for the medium angle grain boundary to local deviations in the boundary conditions.

The photogrammetric method used in the experiment to characterize the strain can only provide information about the deformation at the surface of the bicrystal samples. In order to better understand the micro-mechanical behavior of the entire bicrystal, Fig. 10 shows for the three bicrystals series of seven subsequent through-thickness sections of the equivalent total strain along the Z- or, respectively, ND direction.

An interesting result from these inner sections is the observation that in the small angle bicrystal the grain boundary has been penetrated by a deformation band. Although no specific symmetries can be observed in the first section (neither in the simulation nor in the experiment), localized deformation zones proceed from the lower crystal into the upper one along the ND direction. The middle section reveals an anti-symmetric deformation pattern.

The comparison between the three bicrystals shown in Fig. 10 reveals that the specimen with the small angle grain boundary (7.4°) does not show a substantial grain boundary resistance against the penetration of plastic slip in the form of deformation bands from one crystal into the other. The other two bicrystal samples with larger misorientation angles (15.9°, 33.2°) between the abutting crystals show stronger resistance against deformation penetration. The bicrystal with the large angle grain boundary (33.2°) reveals a strongly deformed zone in the upper grain in the simulations. In the lower grain a less heavy deformed zone begins from the back layer and decays towards the front layer. The bicrystal with the medium angle grain boundary (15.9°) reveals a similar distribution of the strain.

6.1.2. Comparison of the experimental and simulated textures

Fig. 11 shows the {1 1 1} pole figures for the three bicrystals as obtained from the experiments and simulations with

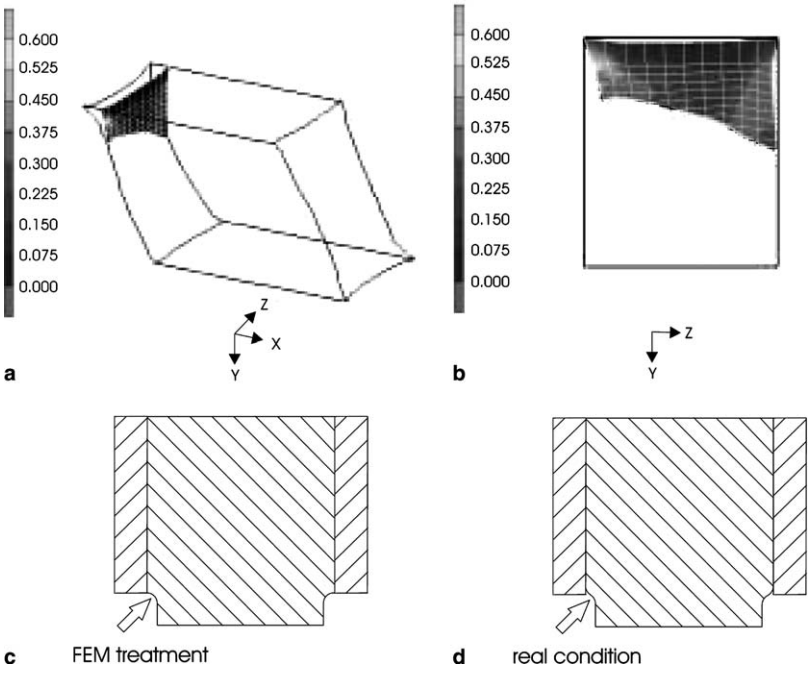

Fig. 9. Deviation of the boundary conditions of the finite element calculation with respect to the boundary conditions in the experiment: (a) position of cut; (b) shape change in the plane shown in (a); (c) modified boundary condition used in the simulation; (d) boundary conditions in the real experiment (schematic).

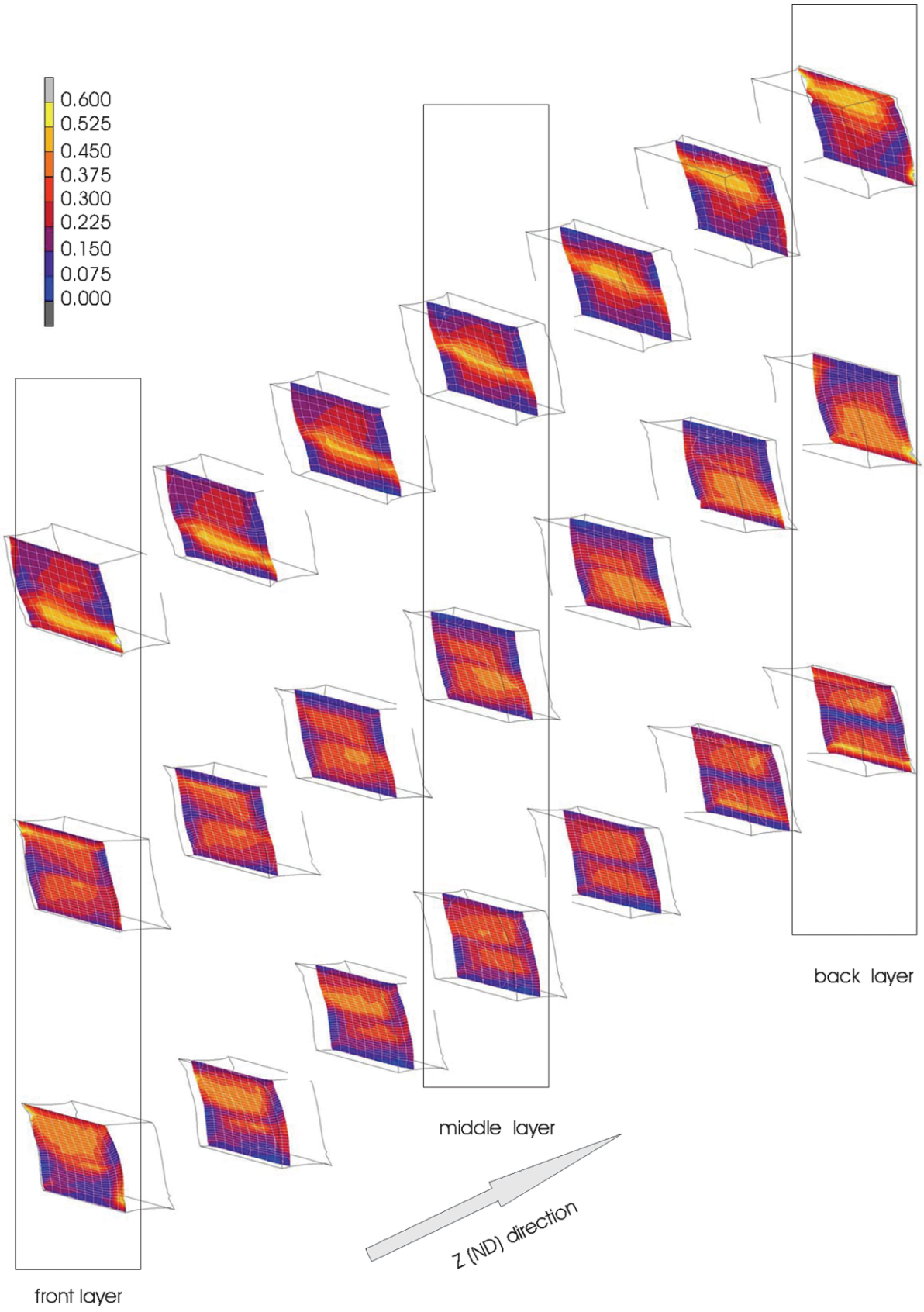

Fig. 10. Von Mises strain distribution in subsequent sections along the Z-axis (ND) as obtained from the simulations. The first row shows the results for the simulations for the bicrystal with the 7.4° grain boundary; the middle row shows the results for the simulations for the bicrystal with the 15.9° grain boundary; the bottom row shows the results for the simulations for the bicrystal with the 33.2° grain boundary. In the front layer the von Mises strain was also measured in experiments as shown in the previous diagrams.

a conventional local model and with the new nonlocal model (50% shear deformation).

The experimental pole figures show reorientation zones with a strong Z (ND) rotation axis which is common to both abutting crystals for all three bicrystal specimens. The scatter of the texture is rather weak in all samples, i.e., the reorientation took place rather homogeneously throughout the crystal when considering that the two abutting orientations were not stable in all three cases under the load imposed. The scatter is due to minor differences in the reorientation rates (similar rotation direction) which originate from local differences in the accumulated strain as is evident from von Mises strain diagrams shown before.

The texture predictions which were obtained by using the local viscoplastic constitutive model (Fig. 11(d)–(f)) show a rather large orientation scatter in all three cases. The texture spread substantially exceeds the scatter observed in the experiments. A distinction between the texture evolution in the two abutting crystals is not possible, i.e., the character of a bicrystal pole figure is lost. This observation matches the strain distributions which were made when using the viscoplastic constitutive law. These data also did not show any influence of the grain boundary on the micro-mechanical behavior except for the case of the large angle grain boundary with 33.2° misorientation where the kinematics of the interface prevailed in terms of the change in the Schmid factor across the boundary.

The texture predictions obtained by the use of the joint nonlocal dislocation and grain boundary constitutive model (Fig. 11(g)–(i)) reveal much smaller orientation scatter and smaller reorientation rates when compared to the simulations obtained by the local phenomenological model

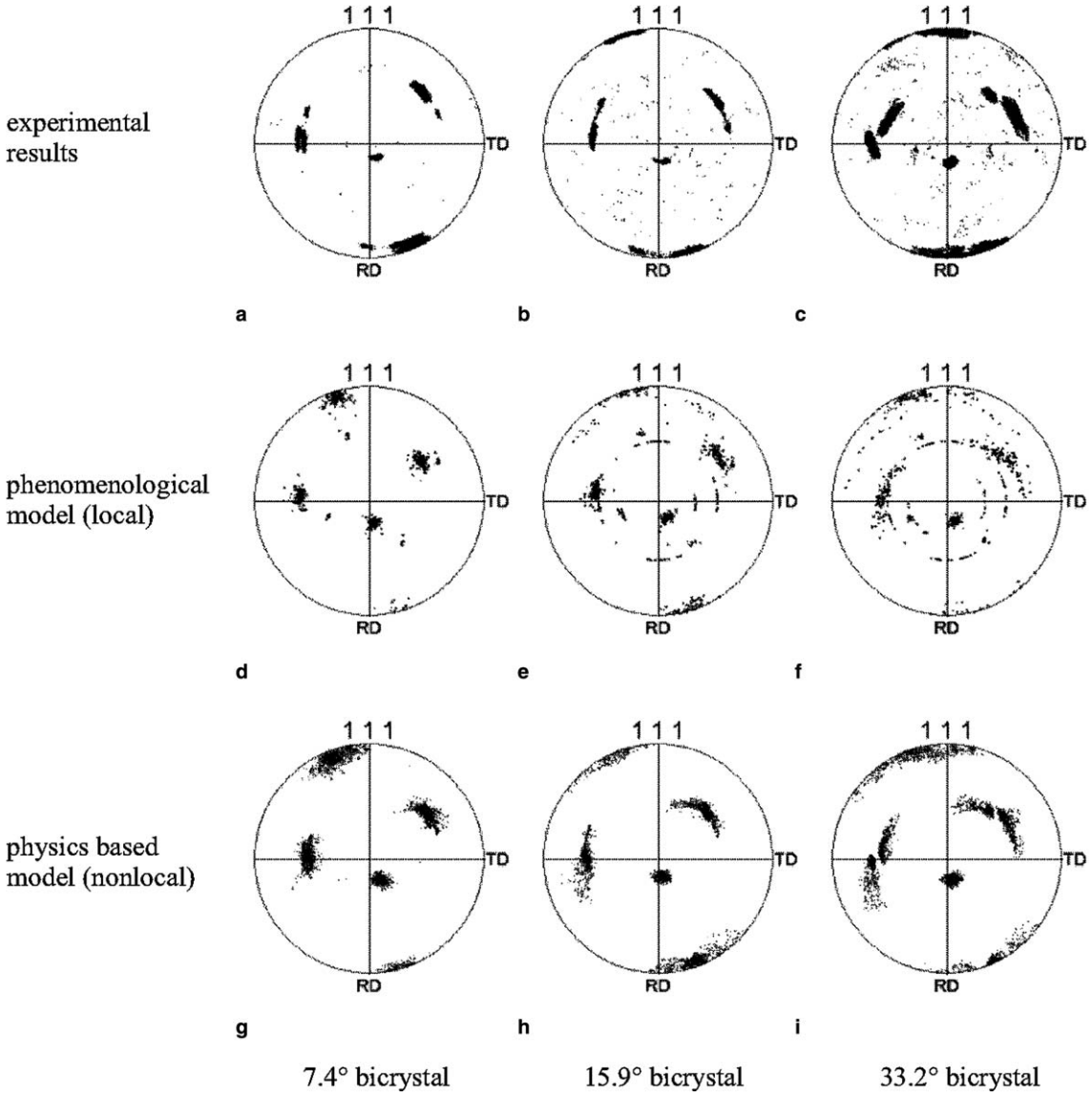

Fig. 11. Texture comparison for the simple shear tests conducted with three bicrystals: (a, b, c) experimental textures; (d, e, f) phenomenological local model; (g, h, i) dislocation and grain boundary nonlocal model; (a, d, g) bicrystal with small angle grain boundary (7.4°); (b, e, h) bicrystal with medium angle grain boundary (15.9°); (c, f, i) bicrystal with large angle grain boundary (33.2°).

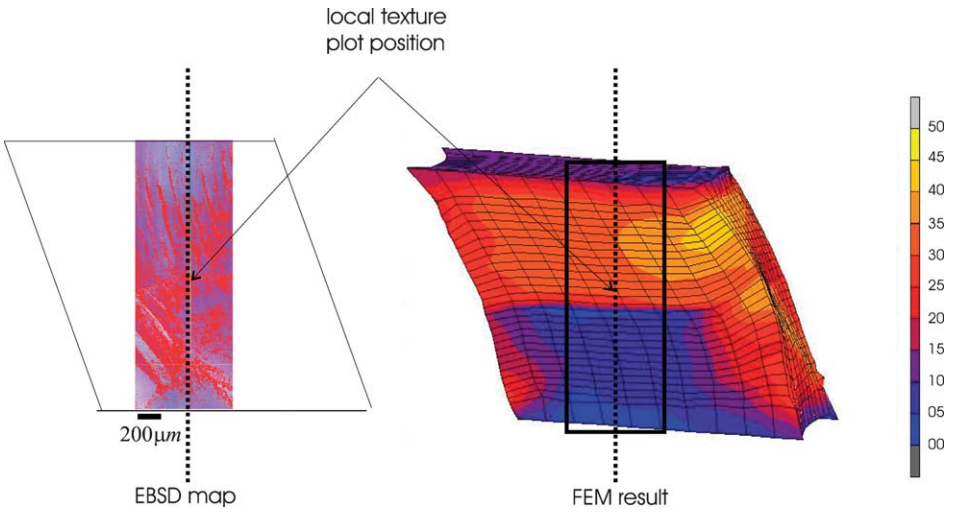

Fig. 12. Positions of the path plot for the local orientation comparison between experiment and numerical simulation. Bicrystal with large angle grain boundary (33.2°) after 50% shear deformation. Red areas in the electron backscatter diffraction map indicate that no orientation could be determined owing to the large deformation. The FEM figure shows the calculated misorientation.

(Fig. 11(d)–(f)). The simulated textures are in excellent accord with the experimental pole figures.

We explain this smoothing effect on the texture evolution mainly in terms of the influence of the geometrically necessary dislocations which act twofold: First, their necessary accumulation in conjunction with the generation of orientation gradients introduces a direct mechanical resistance to the further deformation of the material points affected by such gradients in terms of the increase in the overall local dislocation density. The second aspect (coupled to the first one) is the resulting constitutive tendency of the nonlocal model to reduce the difference in lattice rotation between neighboring material points. This means that the implicit introduction of the geometrically necessary dislocations imposes a strong penalty or, respectively, drag force against lateral gradients in the reorientation rates.

The {1 1 1} pole figures shown in Fig. 11(c) and (i) reveal that the projected orientation points cluster in the form of two groups, while in (f) this effect is less pronounced. This is attributed to the influence of the grain boundary on the texture evolution, in particular to the anisotropy of the modeled resistance of the grain boundaries to different slip systems.

The influence of the nonlocal and of the grain boundary model on the overall reduction in the rate at which the deformation textures evolve is a long standing problem in texture research since many classical texture models (including the crystal plasticity finite element approach) suffer from the drawback that the predicted textures are two sharp and the predicted evolution rates are often too high when compared to experiments.

6.1.3. Comparison of the local orientation

In the preceding section we showed how the new model improves the orientation prediction. However, pole figures only give a statistical impression of the texture evolution. The ultimate goal of any micro-structural model has to be the correct prediction of the local mechanics and micro-structures. We, therefore, compare the local misorientation with respect to the initial orientation along one exemplary line crossing the sample from top to bottom as indicated in Fig. 12, see Fig. 13. Again we observe an excellent agreement between the experimental and the simulated values. The strongest deviations in the misorientation are found near the sample edges, which can be attributed to the non-perfect boundary conditions of the FE model discussed above.

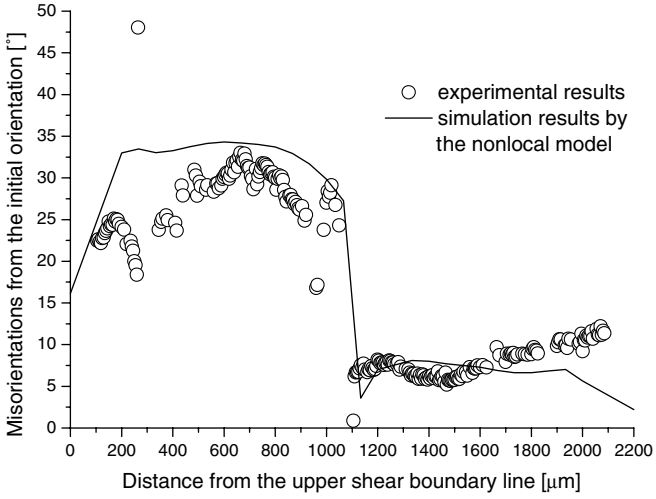

Fig. 13. Comparison of the local misorientation showing experimental and numerical results for the bicrystal with the large angle grain boundary (33.2°) after 50% shear deformation.

7. Conclusions

In an extension of the nonlocal dislocation model suggested in Ref. [1], the current paper introduced a novel constitutive law which accounts for the interaction between

mobile dislocations and grain boundaries in a crystal plasticity finite element framework. The theoretical approach is based on corresponding experimental findings which have been reported in the literature.

The grain boundary mechanism is introduced via an additional activation energy barrier into the rate equation for the slip of mobile dislocations in the vicinity of grain boundaries. The energy barrier is derived by using a geometrical model for thermally activated dislocation penetration events through grain boundaries. The model takes full account of the geometry of the grain boundaries and of the Schmid factors of the critically stressed incoming and outgoing slip systems.

A special grain boundary element was introduced to practically implement the new approach into numerical simulations of three bicrystals with a small, medium and large angle flat grain boundary, respectively. The predictions were compared to experiments (von Mises equivalent total strain, textures) for the case of simple shear.

The result show three main effects which arise from the new model and provide excellent agreement between theory and experiment. These are the accumulation of geometrically necessary dislocations and the resulting pronounced local hardening in front of grain boundaries, the resistance against slip penetration across the grain boundaries, and the reduction of the orientation spread and of the rotation rates in the vicinity of grain boundaries (owing to the effect of the interfaces) and in the crystal interiors (owing to the effect of the geometrically necessary dislocations).

The simulations and experiments clearly show that the classical kinematic treatment of grain boundaries, which is automatically included in all crystal plasticity FE models owing to the change in the Schmid factor across the interfaces is not sufficient to adequately reproduce the micromechanics associated with the presence of grain boundaries.

Acknowledgment

The authors thank Professor G. Gottstein for valuable discussions.

References

[1] Ma A, Roters F, Raabe D. A dislocation density based constitutive model for crystal plasticity FEM including geometrically necessary dislocations. Acta Mater 2006;58:2169–79.
[2] Gao H, Huang Y. Geometrically necessary dislocation and size-dependent plasticity. Scripta Mater 2003;48(2):113–8.
[3] Nye JF. Some geometrical relations in dislocated crystals. Acta Metall 1953;1:153–62.
[4] Zaefferer S, Kuo J-C, Zhao Z, Winning M, Raabe D. On the influence of the grain boundary misorientation on the plastic deformation of aluminum bicrystals. Acta Mater 2003;51(16):4719–35.
[5] Clark WAT, Wagoner RH, Shen ZY, Lee TC, Robertson IM, Birnbaum HK. On the criteria for slip transmission across interfaces in polycrystals. Scripta Metallurgica et Materialia 1992;26(2):203–6.
[6] Evers LP, Parks DM, Brekelmans WAM, Geers MGD. Crystal plasticity model with enhanced hardening by geometrically necessary dislocation accumulation. J Mech Phys Solids 2002;50(11):2403–24.
[7] Arsenlis A, Parks DM. Modeling the evolution of crystallographic dislocation density in crystal plasticity. J Mech Phys Solids 2002;50(9):1979–2009.
[8] Kalidindi SR, Bronkhorst CA, Anand L. Crystallographic texture evolution in bulk deformation processing of fcc metals. J Mech Phys Solids 1992;40:537–69.
[9] Beaudoin AJ, Dawson PR, Mathur KK, Kocks UF. A hybrid finite element formulation for polycrystal plasticity with consideration of macrostructural and microstructural linking. Int J Plasticity 1995;11:501–21.
[10] Raabe D, Sachtleber M, Zhao Z, Roters F, Zaefferer S. Micromechanical and macromechanical effects in grain scale polycrystal plasticity experimentation and simulation. Acta Mater 2001;49(17):3433–41.
[11] Sachtleber M, Zhao Z, Raabe D. Experimental investigation of plastic grain interaction. Mater Sci Eng A 2002;336(1–2):81–7.
[12] Roters F, Wang Y, Kuo J-C, Raabe D. Comparison of single crystal simple shear deformation experiments with crystal plasticity finite element simulations. Adv Eng Mater 2004;6(8):653–6.
[13] Zhao Z, Radovitzky R, Cuitio A. A study of surface roughening in fcc metals using direct numerical simulation. Acta Mater 2004;52(20):5791–804.
[14] Shen Z, Wagoner RH, Clark WAT. Dislocation pile-up and grain boundary interactions in 304 stainless steel. Scripta Metall 1986;20(6):921–6.
[15] Kehagias T, Komninou P, Dimitrakopulos GP, Antonopoulos JG, Karakostas T. Slip transfer across low-angle grain boundaries of deformed titanium. Scripta Metallurgica et Materialia 1995;33(12):1883–8.
[16] Livingston JD, Chalmers B. Multiple slip in bicrystal deformation. Acta Metall 1957;5:322–7.
[17] Lee TC, Robertson IM, Birnbaum HK. An in situ transmission electron microscope deformation study of the slip transfer mechanisms in metals. Metall Trans 1990;21A:2437–47.
[18] Gottstein G, Shvindlerman LS. Grain boundary migration in metals – thermodynamics, kinetics, applications. Boca Raton, FL: CRC Press; 1999.
[19] Sutton AP, Baluffi RW. Interfaces in crystalline materials. Oxford: Clarendon Press; 1995.
[20] Read WT, Shockley W. Dislocation pile-up and grain boundary interactions in 304 stainless steel. Phys Rev B 1950;78:275.
[21] Ma A, Roters F. A constitutive model for fcc single crystals based on dislocation densities and its application to uniaxial compression of aluminium single crystals. Acta Mater 2004;52(12):3603–12.
[22] MSC. Marc user's manual 2003, User Subroutines and Special Routines, vol. D; 2003.
[23] Kuo J-C. Mikrostrukturmechanik von Bikristallen mit Kippkorngrenzen. PhD thesis, RWTH Aachen; 2004.